Spinal cord stimulation alleviates motor deficits in a primate model of Parkinson disease.

Santana, Maxwell B; Halje, Pär; Simplício, Hougelle; Richter, Ulrike; Freire, Marco Aurelio M; Petersson, Per; Fuentes, Romulo; Nicolelis, Miguel A L

Published in:
Neuron

DOI:
10.1016/j.neuron.2014.08.061

2014

Spinal Cord Stimulation Alleviates Motor Deficits in a Primate Model of Parkinson's disease

Maxwell B. Santana[1,7+], Pär Halje[2+], Hougelle Simplício[1,8], Ulrike Richter[2], Marco Aurelio M. Freire[1], Per Petersson[2†], Romulo Fuentes[1†], and Miguel A.L. Nicolelis[1,3,4,5,6†*]

[1]Edmond and Lily Safra Institute of Neuroscience of Natal, 590660 Natal, Brazil.

[2]Integrative Neurophysiology and Neurotechnology, Neuronano Research Center, Department of Experimental Medical Sciences, Lund University, BMC F10, S-221 84 Lund, Sweden.

[3]Biomedical Engineering, Duke Univ., Durham, NC 27708, U.S.A.

[4]Ctr. for Neuroengineering, Duke Univ., Durham, NC 27708, U.S.A.

[5]Dept. of Neurobiology, Duke Univ., Durham, NC 27708, U.S.A.

[6]Dept. of Psychology and Neuroscience, Duke Univ., Durham, NC 27708, U.S.A.

[7]Psychobiology, Federal Univ. of Rio Grande do Norte, Natal, Brazil

[8]State Univ. of Rio Grande do Norte, Natal, Brazil

*Correspondence to: nicoleli@neuro.duke.edu

+These two authors contributed equally to this work

†This study was conducted in a joint effort by these three principle investigators

Summary

Although deep brain electrical stimulation can alleviate the motor symptoms of Parkinson's disease (PD), just a small fraction of PD patients can take advantage of this procedure due to its invasive nature. A significantly less invasive method - epidural spinal cord stimulation (SCS) – has been suggested as an alternative approach for symptomatic treatment of PD. However, the mechanisms underlying motor improvements through SCS are unknown. Here, we show that SCS reproducibly alleviates motor deficits in a primate model of PD. Simultaneous neuronal recordings from multiple structures of the cortico-basal ganglia-thalamic loop in PD monkeys revealed abnormal highly synchronized neuronal activity within each of these structures and excessive functional coupling among them. SCS disrupted this pathological circuit behavior in a manner that mimics the effects caused by pharmacological dopamine replacement therapy or deep brain stimulation. These results suggest that SCS should be considered as an additional treatment option for PD-patients.

Introduction

Chronic electrical stimulation of subcortical brain structures, a procedure known as deep-brain stimulation (DBS), has become an important complement to dopamine replacement therapy in the symptomatic treatment of Parkinson's disease (PD) (Benabid et al., 1987). However, partially because of the highly invasive nature of this surgical procedure (Morgante et al., 2007) and its need for additional complex and costly technologies, only a small fraction of all PD patients that could possibly benefit from this therapy are actually eligible for implantation. In this context, the recent demonstration that electrical epidural spinal cord stimulation (SCS) alleviates akinesia in rodent models of PD (Fuentes et al., 2009) and reduces motor symptoms in patients (Agari and Date, 2012; Fénelon et al., 2011; Hassan et al., 2013; Landi et al., 2012) is a significant finding since SCS, unlike DBS, is minimally invasive. Following the initial report on rodent PD-models, SCS has been evaluated for treatment of PD in a few clinical case studies. Results of these studies range from no measurable improvements in two patients (Thevathasan et al., 2010) to significant symptomatic relief (Agari and Date, 2012; Fénelon et al., 2011; Hassan et al., 2013; Landi et al., 2012) in 19 patients. More importantly, in some cases SCS achieved PD symptom relief equivalent to the best effects obtained by pharmacological treatment (Fénelon et al., 2011). At present, the underlying causes for the different outcomes in these preliminary clinical studies are not known, but variations in electrode design, spinal cord implantation location, and choice of stimulation parameters have been suggested as possible contributing factors (Fuentes et al., 2010; Nicolelis et al., 2010). One way to optimize the application of this potential therapy for PD is to establish what neurophysiological changes are associated with the relief of symptoms, and to evaluate how these changes can be most effectively induced. Here, we have addressed these questions by characterizing the behavioral and neurophysiologic SCS effects in 6-OHDA (6-hydroxydopamine) lesioned marmoset monkeys (*Callithrix jacchus*), a primate model of PD.

Results

Using previously described procedures (Annett et al., 1992; Mitchell et al. 1995), five adult male marmosets were rendered parkinsonian through 6-OHDA stereotactic micro-injections in the medial forebrain bundle (MFB) of either one (n=2) or both hemispheres (n=3). Injections resulted in neurodegeneration of the midbrain dopaminergic neurons projecting to the forebrain in the lesioned hemispheres, as assessed *post mortem* through immunohistochemical quantification of tyrosine hydroxylase (Figure S1). In lesioned animals, the number of dopaminergic neurons in the midbrain was reduced to 42±23% of the values observed in control animals. In addition, axonal terminal staining density in the caudate-putamen decreased to 44±10% of the levels seen in normal subjects. Severity of Parkinsonism was regularly examined in all marmosets using manual scoring of a wide range of clinical signs/deficits (see Supplemental Experimental Procedures and Movie S1 for details) and automated quantification of spontaneous motor behavior. On average, spontaneous locomotion was reduced to about a fourth of pre-lesion activity, and PD-signs approached the maximum score (mean±SD: 75±29%) in all the eight categories assessed (Bankiewicz et al., 2001; Verhave et al., 2009).

Once PD clinical signs had been confirmed, animals were implanted with bipolar epidural SCS electrodes positioned symmetrically over the dorsal midline of the spinal cord at high thoracic level (T_3-T_4). Four of the five animals (two with bilateral and two with unilateral MFB lesions) were also chronically implanted with microelectrode arrays/bundles in both hemispheres for subsequent record of neuronal ensemble activity (both single units and LFPs; Figure S2). These implants targeted multiple structures in each animal, including: the primary motor cortex (MI), putamen (Put), the sub-thalamic nucleus (STN), globus pallidus pars externa (GPe) and interna (GPi), and the ventrolateral (VL) and ventral posterolateral (VPL) thalamic nuclei. In the two unilateral-lesion animals, instead of globus pallidus, parts of primary somatosensory

cortex (SI) were implanted. Prior to SCS, all animals were also subjected to acute pharmacological inhibition of dopamine synthesis (s.c. injections of alpha-methyl-p-tyrosine [AMPT] 2x240mg/kg) to further aggravate the PD signs.

To avoid SCS current intensities that could be experienced as uncomfortable, before each stimulation session the intensity of each stimulation frequency was adjusted and set to 1.7 times the minimum intensity at which any behavioral response could be consistently detected (small postural changes, head or neck movements). Overall, as previously reported in rodents (Fuentes et al., 2009), we observed that SCS induced a clear alleviation of motor impairment in monkeys that exhibited severe clinical PD signs. Because the stimulation frequencies used in this study (range 4-300 Hz) proved equally effective, the analysis of the SCS effects, both behavioral and electrophysiological, were performed by pooling all the frequencies, unless otherwise stated. All recordings/stimulation sessions were performed in freely behaving animals in a transparent acrylic box. Based on our automated image analysis of digital videos obtained from multiple cameras during neuronal recording sessions, SCS induced a 221% increase in general motility of trunk, head, limbs and tail ($p<0.05$, Wilcoxon signed rank test, Figure 1A), a 192% increase in the frequency of bouts of spontaneous locomotion ($p<0.001$, two-proportional z-test, Figure 1B) and a 144% increase in the duration of locomotion periods ($p<0.05$, Wilcoxon rank sum test, Figure 1C). These improvements resulted in a 243% increase in the total distance covered ($p<0.05$, Wilcoxon rank sum test, Figure 1D) by the monkeys. Remarkably, SCS induced a preferential increase in the fraction of faster locomotion components indicating a specific reduction of bradykinesia, ($p<0.05$, Kolmogorov-Smirnov test of difference in speed histogram distributions, Figure 1E). Overall, the resulting distance covered in locomotive behavior was practically normalized by SCS (on average 91% of intact values, but locomotion differed somewhat in that stimulated animals tended to extend bout duration [628%] while reducing the frequency [11%] compared to the intact state).

The improvements in motor disability were also assessed by an observer blinded to stimulation conditions that rated specific clinical signs, such as freezing, hypokinesia, bradykinesia, coordination, gait, posture, and gross and fine motor skills, during the OFF and ON periods. The motor deficits that exhibited the highest reduction during SCS were freezing (31%), hypokinesia (23%), posture (23%) and bradykinesia (21%). Overall, the PD-score showed on average a significant reduction of 18.4 ± 13.9% ($p<0.001$, Wilcoxon signed rank sum test [including all five subjects], Figure 1F; Figure S1).

In addition to the general clinical improvements observed in all monkeys, in a few instances SCS resulted in an extraordinary functional recovery. An example of this is shown in Figure 1G, where a severely parkinsonian animal, who reached the maximum PD score on all clinical signs rated, showed a dramatic improvement during SCS. This allowed the animal to find and retrieve a food item with no difficulty whatsoever (See Movie S2).

Chronic, multi-site neuronal extracellular activity was analyzed both in terms of changes in single neuron's firing patterns and at the level of local field potentials (LFPs). We observed that SCS induced changes in neural populations throughout the cortico-basal ganglia-thalamic loop in parkinsonian animals (Figure 2A). As shown in Figures 2B and 2C, the most noticeable effect was the suppression of LFP power in a frequency interval roughly spanning the beta-band (8-20 Hz), which was abnormally strong in all PD monkeys (respective peak power frequencies for the four subjects were 10, 11, 12, and 15 Hz; Figure S3A) (Stein and Bar-Gad, 2013). This suppression of LFP oscillations was observed in all animals and, notably, in all parts of the cortico-basal ganglia-thalamic loop (although it did not reach significance level, $p<0.05$, in GPe when comparing averaged power spectra; Figures 2B and 2C, $p<0.05$, Wilcoxon rank sum test on band power 8-20 Hz). In agreement with the behavioral effects, beta suppression could be obtained using both low- and high-frequency SCS paradigms

with approximately equal efficacy (average LFP power spectra ON/OFF stimulation for all animals and frequencies are presented in Figure 2B).

Next, we examined the effects of SCS on single unit activity. Overall, about one third of the neurons recorded in the lesioned hemispheres displayed significant changes in firing rates associated with SCS. In contrast to the effect on LFP and motor behavior, SCS modulation of neuronal firing rate differed markedly according to the stimulation frequency (Figure 3A, see also Figure S3C). While stimulation at low-frequencies (4-20 Hz) caused mostly excitatory neuronal responses, inhibitory firing modulation predominated during high-frequency stimulation (80-300 Hz; Pearson correlation between the ratio of inhibitory/excitatory responses and stimulation frequency was: MI, $r=0.96$, $p<0.01$; PU, $r=0.74$, $p<0.05$; VP, $r=0.94$, $p<0.01$; VL, $r=0.76$, $p<0.05$; STN, $r=0.92$, $p<0.01$; GPe and GPi not significant, Figure 3B).

Consistent with the LFP oscillatory activity, we observed a large fraction of neurons with beta oscillatory firing in the OFF period (Figure 3C) that was partially suppressed during the SCS ON period (Figure 3D, E, and S2). In total, 152 neurons out of 273 (56%) from the lesioned hemispheres displayed significant beta-range (8-16 Hz) rhythmic firing patterns during the OFF periods ($p<0.01$, as compared to spectra computed from equivalent random spike trains). Of these 152 neurons, 39 (26%) significantly decreased their beta rhythmicity during the SCS ON period. The change in beta power for all units with significant rhythmic activity in the beta range is summarized in Figure 3F.

Taken altogether, these data suggest that SCS-induced motor deficit relief is primarily associated with the disruption of synchronized oscillatory activity rather than with specific changes in firing rate. However, because cortico-basal ganglia activity is known to be strongly influenced by behavioral state, neurophysiologic changes could also result, to some extent, from secondary changes in animal motor behavior. Therefore, to further clarify how SCS induces neurophysiologic changes that may

cause symptomatic relief, we compared the neuronal activity patterns from the lesioned hemisphere during SCS, in the two hemi-lesioned animals, to either the patterns of the intact hemisphere or to the lesioned hemisphere following L-DOPA treatment (s.c. 15 mg/kg with Benserazide 6.25 mg/kg). Recordings were split into 4 second epochs that were classified as either active or inactive states based on automatically quantified motor activity. To facilitate comparisons between states, two separate indices were constructed. First, two vectors were created summarizing the mean differences [parkinsonian vs. intact state] and [parkinsonian vs. L-DOPA treated state], respectively, in two multi-dimensional parameter spaces - spectral LFP power and firing rate per structure. Each recorded epoch could then be represented as a point in the parameter spaces and be quantitatively compared to the intact or L-DOPA treated state by geometrical projection onto these vectors. Using this metric, it was evident that SCS treatment caused a shift towards healthy brain activity patterns resembling the effect of L-DOPA treatment. This effect was observed only for the analysis of LFP spectral power and not for neuronal firing rates (Figure S3B). Importantly, this shift could not be explained as a secondary effect due to an active or inactive behavioral state since a two-way ANOVA, employed to estimate the relative effect-size of SCS compared to that of behavioral state, showed that only 2.9%and 0.8% of the total variance (eta-squared; using the metric for the intact and L-DOPA treated state, respectively) could be attributed to behavioral state change, whereas the effect of SCS treatment explained 13.4% and 10.8% of the total variance.

Consequently, the main effect shared by both SCS and L-DOPA treatment appears to be the suppression of the excessive neuronal population synchronization associated with the parkinsonian state. Although it is not clear how coordinated low-frequency activity patterns arise in PD, it is possible that an altered functional coupling between the circuit elements of the cortico-basal ganglia-thalamic loop may be a key underlying factor (Williams et al., 2002). To test this idea, we computed the coherence

of the LFP signals between pairs of different neural structures as an indirect measure of their functional connectivity. In the 6-OHDA lesioned dopamine-depleted hemispheres, we found strong coherence between pairs of structures, but only in the parkinsonian low-frequency range (8-15 Hz) (Fig. 4A, black traces). Importantly, like the L-DOPA treatment, SCS reduced the beta coherence (Fig. 4A red trace), leading to a significant functional decoupling between the different structures. This suggests that SCS brings the functional connectivity of the cortico-basal ganglia-thalamic circuit closer to the normal state of the intact brain. Indeed, this decoupling of parkinsonian LFP oscillations in the beta band was observed between all the recorded structures and was found to be very similar following L-DOPA and SCS (Fig. 4B).

To further explore the underlying mechanisms whereby SCS alters network activity, we recorded neural activity while delivering single or pairs of SCS pulses. These recordings showed that primary somatosensory pathways (VPL and SI) are activated early by SCS and that a disruption of beta oscillations through a phase-reset mechanism appears to cause the observed wide-spread desynchronization in the beta band (Figure S4; Fuentes et al. 2010; Popovych and Tass, 2012).

Discussion

In conclusion, we observed that SCS caused clear clinical improvements in a primate model of PD (comparable to, for example, the reported long-term reduction in UPDRS III score by DBS, ~28%, Follet et al 2010) and in particular for motor signs known to be difficult to treat with DBS. These include deficits in posture, gait and speed of locomotion (Krack and Batir, 2003). Concurrent multi-site neuronal recordings showed that significant behavioral improvements induced by SCS were strongly associated with desynchronization of neuronal activity within the cortico-basal ganglia circuitry and reduction in beta-frequency coherence between structure pairs. We

therefore propose that SCS should be further tested in clinical studies aimed at measuring its long-term efficacy as a less invasive, long-term therapy for PD patients.

Experimental Procedures

Five adult male common marmosets (*Callithrix jacchus*) 300-550g were used in the study. The animals were housed in pairs in cages (1.0 x 1.0 x 2.3 m) in a vivarium with natural light cycle (12/12 hours) and outdoor temperature. All animal procedures were carried out according to approved protocols by AASDAP Ethics Committee and strictly in accordance with the National Institute of Health Guide for the Care and Use of Laboratory Animals (NIH Publications No. 80-23). This project was approved by SISBIO/Brazilian Institute of Environment and Natural Resources under No. 20795-2.

Neurotoxic lesions were inflicted under deep anesthesia. Two μl of 6-OHDA solution (4mg/mL, 0.05% ascorbic acid, saline) were injected into the medial forebrain bundle in (AP/ML/DV): 6.5/1.2/6.0; 6.5/1.2/7.0; 6.5/2.2/6.5; 6.5/2.2/7.5; 6.5/3.2/8.0 (Annett et al., 1992). AP-coordinates were scaled according to the dimensions of the skull of each animal (Stephan et al., 1980).

The following parkinsonian symptoms were assessed in the transparent acrylic box: episodes of freezing, uncoordinated gait, difficulty using fine motor skills, episodes of bradykinesia, hypokinesia, balance impairment, and posture. The assessment methods were based on previously described procedures (Bankiewicz et al., 2001; Campos-Romo et al., 2009; Fahn and Elton, 1987; Verhave et al., 2009) and are thoroughly described in the Supplemental Information. Automatic motion tracking was performed using custom developed software in MATLAB.

Local field potentials (LFPs) and action potentials were recorded using a multi-channel recording system (Plexon Inc.).

Analyses of recorded signals were performed according to previously described methods (Fuentes et al., 2009a; Halje et al., 2012).

The position of the recording electrode positions and the extent of dopaminergic lesions were verified through quantitative tyrosine hydroxylase staining in all animals.

References

Agari, T., and Date, I. (2012). Spinal cord stimulation for the treatment of abnormal posture and gait disorder in patients with Parkinson's disease. Neurol. Med. Chir. (Tokyo). *52*, 470–474.

Annett, L.E., Rogers, D.C., Hernandez, T.D., and Dunnett, S.B. (1992). Behavioural analysis of unilateral monoamine depletion in the marmoset. Brain *115 (Pt 3*, 825–856.

Bankiewicz, K.S., Sanchez-Pernaute, R., Oiwa, Y., Kohutnicka, M., Cummins, A., and Eberling, J. (2001). Preclinical Models of Parkinson's Disease. In Current Protocols in Neuroscience, (John Wiley & Sons, Inc.),.

Benabid, A.L., Pollak, P., Louveau, A., Henry, S., and de Rougemont, J. (1987). Combined (thalamotomy and stimulation) stereotactic surgery of the VIM thalamic nucleus for bilateral Parkinson disease. Appl Neurophysiol *50*, 344–346.

Campos-Romo, A., Ojeda-Flores, R., Moreno-Briseño, P., and Fernandez-Ruiz, J. (2009). Quantitative evaluation of MPTP-treated nonhuman parkinsonian primates in the HALLWAY task. J. Neurosci. Methods *177*, 361–368.

Fahn, S., and Elton, R.L. (1987). Unified Parkinsons Disease Rating Scale. Recent Dev. Park. Dis. *2*, 153–163.

Fénelon, G., Goujon, C., Gurruchaga, J.-M., Cesaro, P., Jarraya, B., Palfi, S., and Lefaucheur, J.-P. (2012). Spinal cord stimulation for chronic pain improved motor function in a patient with Parkinson's disease. Parkinsonism Relat. Disord. *18*, 213–214.

Follett, K.A., Weaver, F.M., Stern, M., Hur, K., Harris, C.L., Luo, P., Marks, W.J., Rothlind, J., Sagher, O., Moy, C., et al. (2010). Pallidal versus subthalamic deep-brain stimulation for Parkinson's disease. N. Engl. J. Med. *362*, 2077–2091.

Fuentes, R., Petersson, P., Siesser, W.B., Caron, M.G., and Nicolelis, M.A.L. (2009). Spinal cord stimulation restores locomotion in animal models of Parkinson's disease. Science *323*, 1578–1582.

Fuentes, R., Petersson, P., and Nicolelis, M. a L. (2010). Restoration of locomotive function in Parkinson's disease by spinal cord stimulation: mechanistic approach. Eur. J. Neurosci. *32*, 1100–1108.

Halje, P., Tamte, M., Richter, U., Mohammed, M., Cenci, M. a., and Petersson, P. (2012). Levodopa-Induced Dyskinesia Is Strongly Associated with Resonant Cortical Oscillations. J. Neurosci. *32*, 16541–16551.

Hassan, S., Amer, S., Alwaki, A., and Elborno, A. (2013). A patient with Parkinson's disease benefits from spinal cord stimulation. J. Clin. Neurosci.

Krack, P., and Batir, A. (2003). Five-year follow-up of bilateral stimulation of the subthalamic nucleus in advanced Parkinson's disease. N. Engl. J. Med. *349*, 1925–1934.

Landi, A., Trezza, A., Pirillo, D., Vimercati, A., Antonini, A., and Sganzerla, E. Pietro (2012). Spinal Cord Stimulation for the Treatment of Sensory Symptoms in Advanced Parkinson's Disease. Neuromodulation *2012*.

Mitchell, I J., Hughes, N., Carroll, C. and B.J. (1995). Reversal of parkinsonian symptoms by intrastriatal and systemic manipulations of excitatory amino acid and dopamine transmission in the bilateral 6-OHDA lesioned marmoset. Behav. Pharmacol. Pharmacol. *6*, 492–507.

Morgante, L., Morgante, F., Moro, E., Epifanio, A., Girlanda, P., Ragonese, P., Antonini, A., Barone, P., Bonuccelli, U., Contarino, M.F., et al. (2007). How many parkinsonian patients are suitable candidates for deep brain stimulation of subthalamic nucleus? Results of a questionnaire. Parkinsonism Relat. Disord. *13*, 528–531.

Nicolelis, M.A., Fuentes, R., Petersson, P., Thevathasan, W., and Brown, P. (2010). Spinal cord stimulation failed to relieve akinesia or restore locomotion in Parkinson disease. Neurology *75*, 1484; author reply 1484–5.

Popovych, O. V, and Tass, P.A. (2012). Desynchronizing electrical and sensory coordinated reset neuromodulation. Front. Hum. Neurosci. *6*, 58.

Stein, E., and Bar-Gad, I. (2013). β oscillations in the cortico-basal ganglia loop during parkinsonism. Exp. Neurol. *245*, 52–59.

Stephan, H. (Heinz), Baron, G. (Georg), and Schwerdtfeger, W.K. (Walter K.. (1980). The brain of the common marmoset (Callithrix jacchus) : a stereotaxic atlas.

Verhave, P.S., Vanwersch, R. a. P., van Helden, H.P.M., Smit, A.B., and Philippens, I.H.C.H.M. (2009). Two new test methods to quantify motor deficits in a marmoset model for Parkinson's disease. Behav. Brain Res. *200*, 214–219.

Williams, D., Tijssen, M., Van Bruggen, G., Bosch, A., Insola, A., Di Lazzaro, V., Mazzone, P., Oliviero, A., Quartarone, A., Speelman, H., et al. (2002). Dopamine-dependent changes in the functional connectivity between basal ganglia and cerebral cortex in humans. Brain *125*, 1558–1569.

Acknowledgments: We are thankful to Tobias Palmér for developing the video tracking software used for automatic quantification of locomotor behavior; Jim Meloy and Gary Lehew for building recording electrodes, Ivani Brys for statistical discussion, Carlos Eduardo Idalino for support with data analysis, Pedro Calvacanti for support in IHC, and Marcelo Carvalho for technical support. This research was supported by The Michael J. Fox Foundation for Parkinson's Research; FINEP 01.06.1092.00; INCEMAQ – Program of National Institutes of Science and Technology of CNPq/MCT; The Swedish Research Council [#325-2011-6441]; Swedish Society for Medical Research; the Olle Engkvist, Parkinson Research, Crafoord, Åke Wiberg, Magnus Bergvall, Kockska and Segerfalk Foundation; NIH Transformative award (R01-NS073125-03). M.S, H.S, P.H., R.F , P.P, and M.A.L.N. designed the experiments; M.S, H.S, R.F., and P.P performed the surgeries; M.S. conducted experiments; M.S. and M.F. performed immunohistochemistry; M.S., P.H., U.R., P.P., R.F., and M.A.L.N. analyzed the data, M.S., P.H, U.R, P.P., R.F., and M.A.L.N. wrote the paper.

Fig. 1. **Spinal cord stimulation alleviates motor symptoms in parkinsonian primates.** (**A**) Average effect on general motility in response to SCS. Each color line represents one recorded animal over all trials. (**B-D**), Average recovery of locomotion: bout distance, bout frequency and duration, respectively (colors represent the four different subjects and asterisks denote significant group differences). (**E**), Reduction in bradykinesia reflected by the preferential recovery of faster movement components in locomotion. (**F**), Average improvements in PD-score in all testing sessions divided by symptom category (mean and SEM shown). (**G**)**,** Example of functional motor improvement from a state of severe Parkinsonism enabling an animal to retrieve food rewards using skilled reaching and grasping movements.

Fig. 2. Spinal cord stimulation alters neuronal activity patterns in basal ganglia circuits. (**A**)**,** Example of parallel changes in LFP power in multiple structures of the cortico-basal ganglia-thalamic loop. For each brain structure, the panel at the right depicts pooled LFP spectrograms (brain slice figures reproduced with permission from Palazzi&Bordier, The Marmoset Brain in Stereotaxic Coordinates, Springer Science+Business Media, LLC). Note the immediate reduction of low-frequency oscillations (beta band) in response to SCS (red bar, stimulation frequency: 4 Hz; color codes denote dB above pink noise background for LFPs). (**B**), Average LFP spectra for all recording sessions normalized to pink noise showing a significant SCS-induced reduction in LFP beta-power in all structures except GPe. (**C**), Changes in normalized firing rates of individual neurons were diverse but, on average, they decreased in response to SCS in GPi and VL.

Fig. 3. Spinal cord stimulation alters the firing rate and rhythmicity of neuronal units in basal ganglia circuits. (**A**), Standardized neuronal firing rate response to different SCS frequencies in multiple structures of the basal ganglia circuits (neurons rank ordered according to responses). (**B**), The fraction of inhibitory responses increased with higher SCS frequencies. (**C**), Autocorrelograms of two single units in MI exemplifying beta-range rhythmic firing pattern in a parkinsonian animal (SCS OFF). (**D**), Autocorrelograms of the same two units showing that the rhythmic spiking is effectively interrupted by SCS. (**E**), The respective power spectra OFF/ON (black/red) for the units shown in C-D. Note the peak (arrow) in the beta-range during the OFF period, which disappears during the ON period. (**F**), Changes in power of rhythmic beta-firing plotted for all 183 units that presented significant beta oscillations either in the OFF or ON period. Colored circles represent the units with significant suppression in beta power during the ON period. Black line denotes equal power in ON and OFF conditions, thus units located to the right of the line display beta suppression.

Fig. 4. Spinal cord stimulation and L-DOPA treatment suppresses multi-structure LFP coherence. (**A**), Example of LFP coherence spectra from one of the hemi-lesioned animals (black trace) showing coherent oscillations restricted to the beta-band in the parkinsonian condition (arrows) that are suppressed by SCS (red trace; bold line and shaded area denote median and interquartile range, stimulation artefacts around 20 and 40Hz have been removed). (**B**), Connectivity diagram representing the pooled LFP coherence in the 8-15Hz range in relation to the 30-40Hz band between all pairs

of electrodes in the different structures (values represent averages from all five recordings in the two hemi-lesioned animals; all changes in beta-to-gamma coherence for SCS ON/OFF are significant $p<0.05$, Wilcoxon rank sum test). Note that the excessive beta-band coherence, represented by the warm colors in the parkinsonian state, is effectively reduced by SCS in the same way as for L-DOPA treatment.

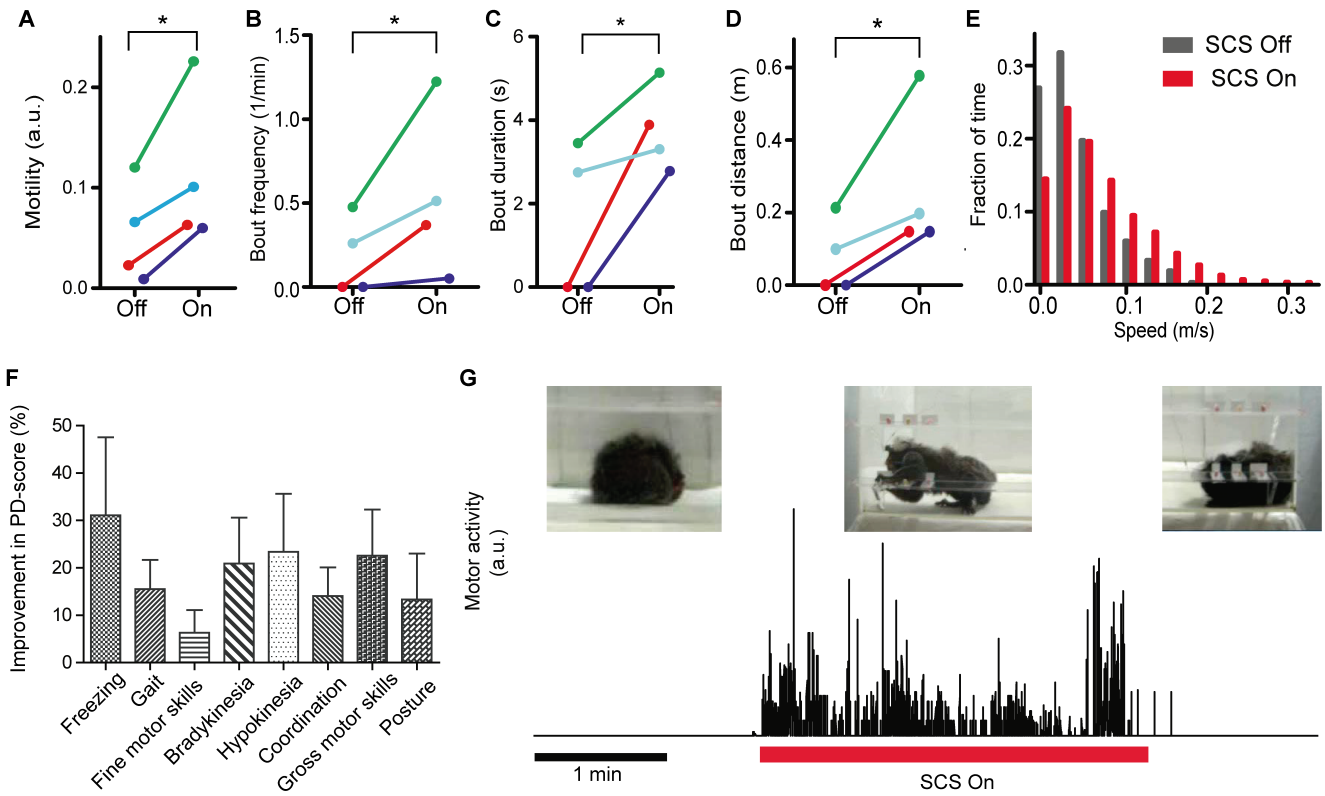
A
Motility (a.u.)
0.0
0.1
0.2
Off
On
*
B
Bout frequency (1/min)
0.0
0.5
1.0
1.5
Off
On
*
C
Bout duration (s)
0
2
4
6
Off
On
*
D
Bout distance (m)
0.0
0.2
0.4
0.6
Off
On
*
E
Fraction of time
0.0
0.1
0.2
0.3
Speed (m/s)
SCS Off
SCS On
F
Improvement in PD-score (%)
0
10
20
30
40
50
Freezing
Gait
Fine motor skills
Bradykinesia
Hypokinesia
Coordination
Gross motor skills
Posture
G
Motor activity (a.u.)
1 min
SCS On

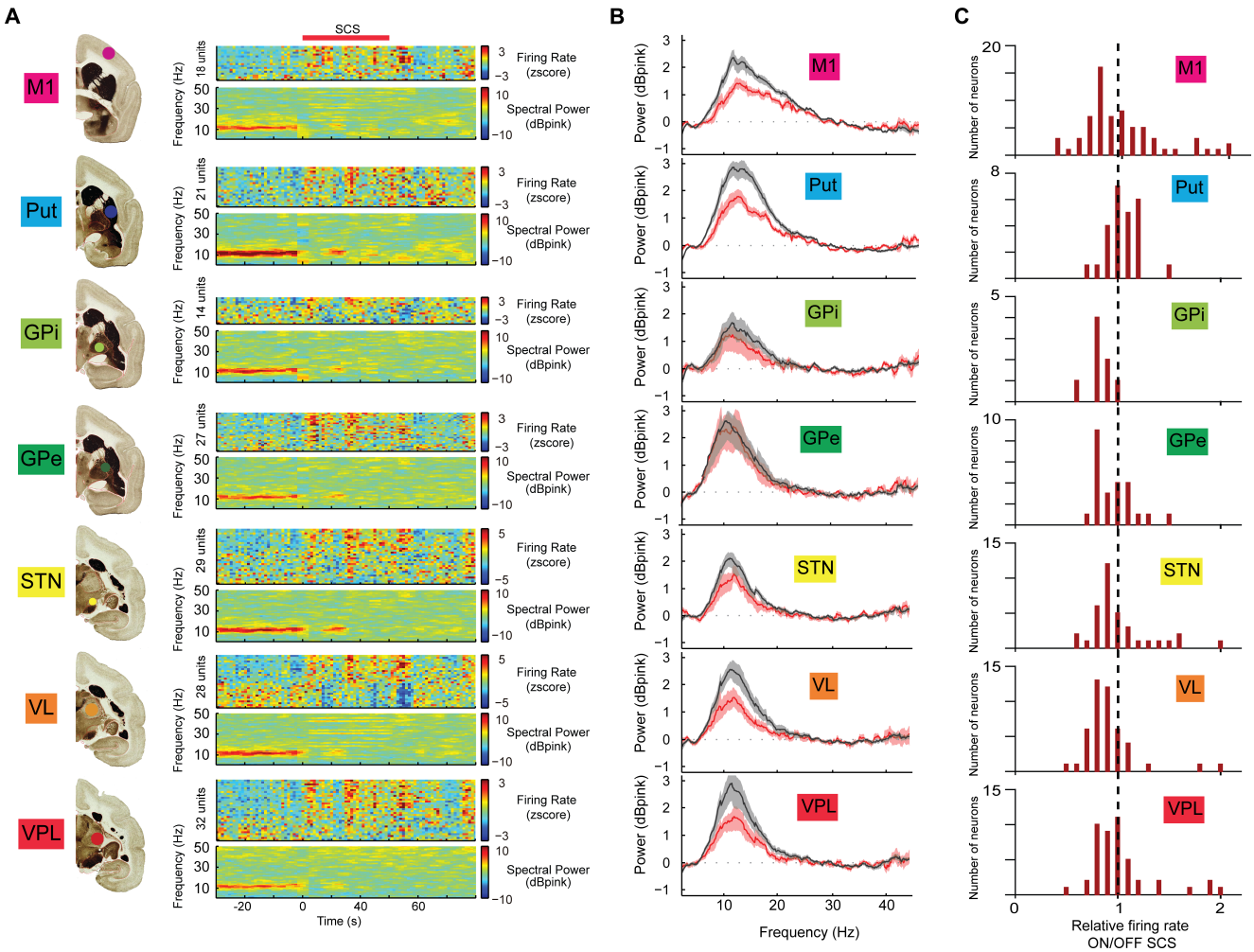
A
B
C
M1
Put
GPi
GPe
STN
VL
VPL
SCS
Frequency (Hz)
18 units
21 units
14 units
27 units
29 units
28 units
32 units
Firing Rate (zscore)
Spectral Power (dBpink)
Time (s)
Power (dBpink)
Frequency (Hz)
Number of neurons
Relative firing rate
ON/OFF SCS

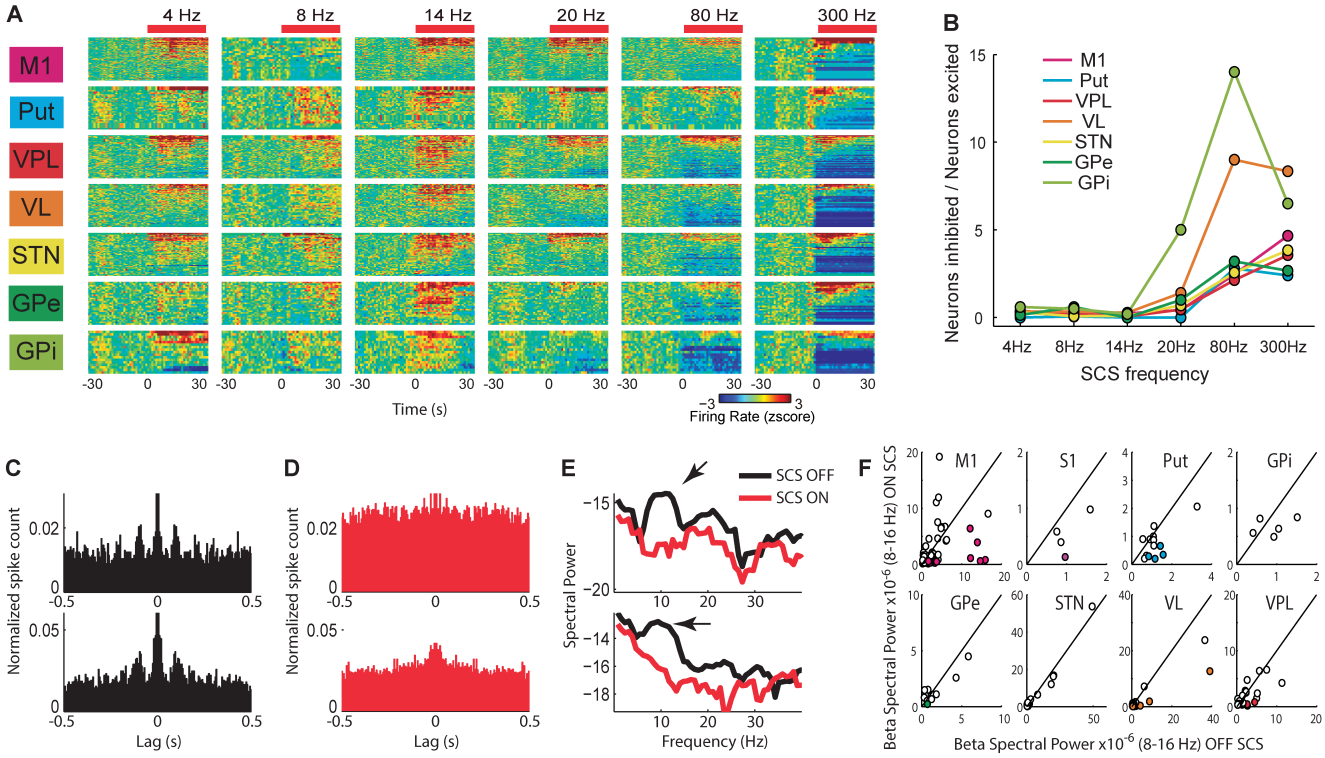
A
4 Hz
8 Hz
14 Hz
20 Hz
80 Hz
300 Hz
M1
Put
VPL
VL
STN
GPe
GPi
-30 0 30
Time (s)
−3 3
Firing Rate (zscore)
B
Neurons inhibited / Neurons excited
15
10
5
0
M1
Put
VPL
VL
STN
GPe
GPi
4Hz 8Hz 14Hz 20Hz 80Hz 300Hz
SCS frequency
C
Normalized spike count
0.02
0
0.05
0
-0.5 0 0.5
Lag (s)
D
Normalized spike count
0.02
0
0.05
0
-0.5 0 0.5
Lag (s)
E
SCS OFF
SCS ON
Spectral Power
−15
−20
−14
−16
−18
10 20 30
Frequency (Hz)
F
M1
S1
Put
GPi
GPe
STN
VL
VPL
Beta Spectral Power x10-6 (8-16 Hz) ON SCS
Beta Spectral Power x10-6 (8-16 Hz) OFF SCS

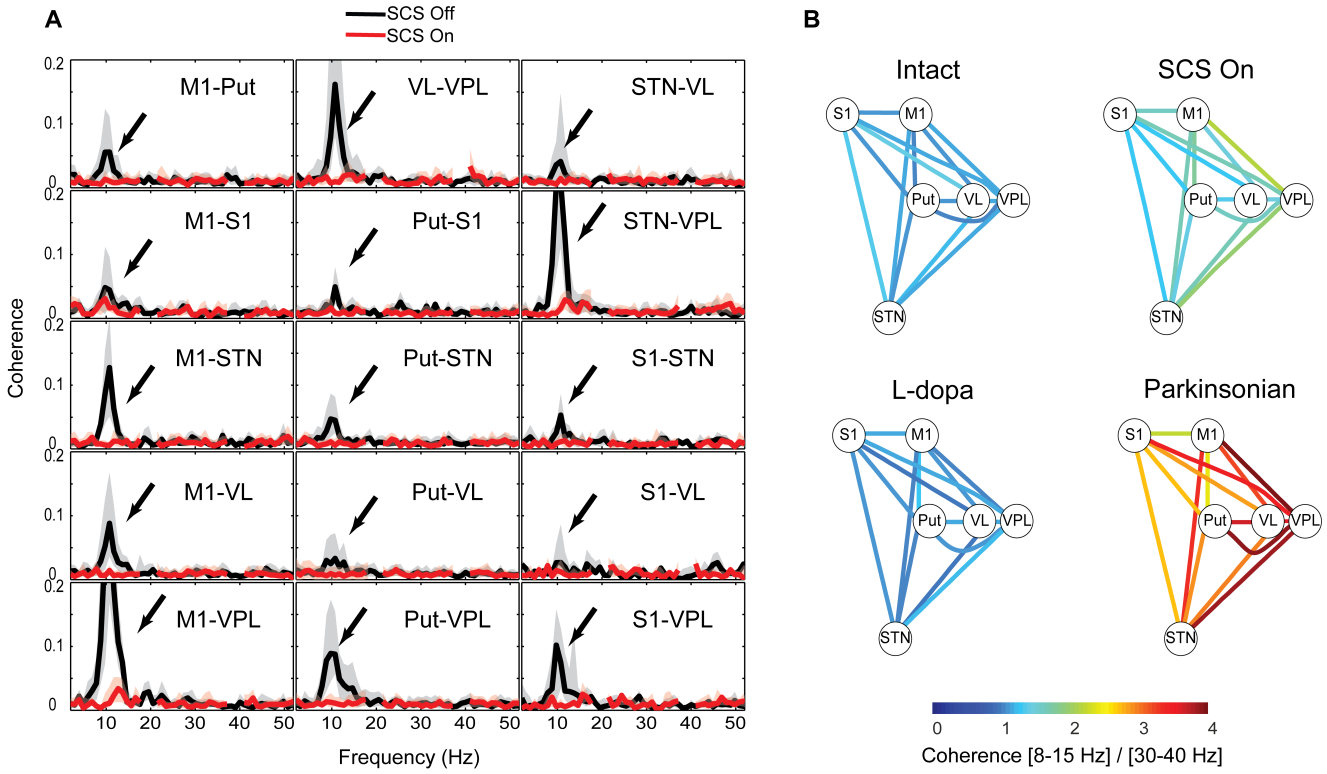
A
SCS Off
SCS On
M1-Put
VL-VPL
STN-VL
M1-S1
Put-S1
STN-VPL
M1-STN
Put-STN
S1-STN
M1-VL
Put-VL
S1-VL
M1-VPL
Put-VPL
S1-VPL
Coherence
0.2
0.1
0
10 20 30 40 50
Frequency (Hz)
B
Intact
SCS On
L-dopa
Parkinsonian
S1
M1
Put
VL
VPL
STN
0 1 2 3 4
Coherence [8-15 Hz] / [30-40 Hz]

Supplemental Information

Spinal Cord Stimulation Alleviates Motor Symptoms in a Primate Model of Parkinson's disease

M. Santana, P. Halje, H. Simplício, U. Richter, M. Freire, P. Petersson, R. Fuentes, and M.A.L. Nicolelis

This PDF file includes:

- Supplemental figures S1- S4
- Supplemental Experimental Procedures
- Supplemental References
- Legends for Movies S1 and S2

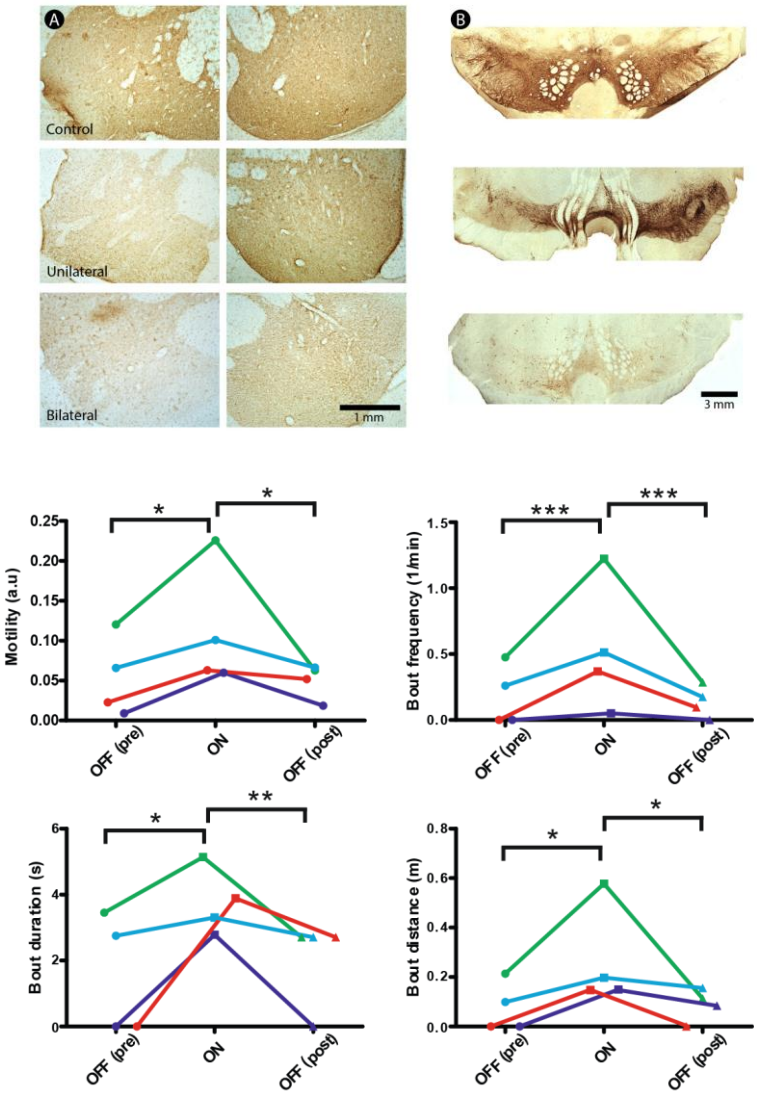

Figure S1, related to Figure 1.
Top. Histological verification of lesions: examples of tyrosine hydroxylase (TH) immunolabeling across striatum (A) and substantia nigra (B) in control and 6-OHDA lesioned animals. Control animals presented an intense labelling in the striatum (putamen and caudate nucleus) and substantia nigra in both hemispheres (top panels). Lesions performed in one hemisphere induced a pronounced loss of labelling in both striatum and substantia nigra on the ipsilateral side (middle panels). In bilaterally lesioned animals both sides were strongly affected, showing a much smaller tissue reaction compared to control (bottom panels). **Bottom.** Behavioral effects do not significantly outlast the stimulation. On average the motility and frequency, duration and distance of locomotion bouts were not significantly different following SCS compared to pre-SCS values suggesting that the immediate effects of SCS assed in these experiments do not outlast the stimulation period. The pre-SCS period was defined as the 30 seconds immediately before SCS on-set, while the post-SCS period was defined as the 30 seconds immediately after SCS off-set. All significant group differences are indicated in the respective panels (omnibus tests [$p<0.05$] were performed, followed by post-tests on all pairs * $p<0.05$, ** $p<0.01$, *** $p<0.001$; Motility: Friedman followed by Wilcoxon signed rank test, Bout frequency: Chi-square test followed by two-proportional z-test, Bout duration and distance: Kruskal-Wallis followed by Wilcoxon rank sum test).

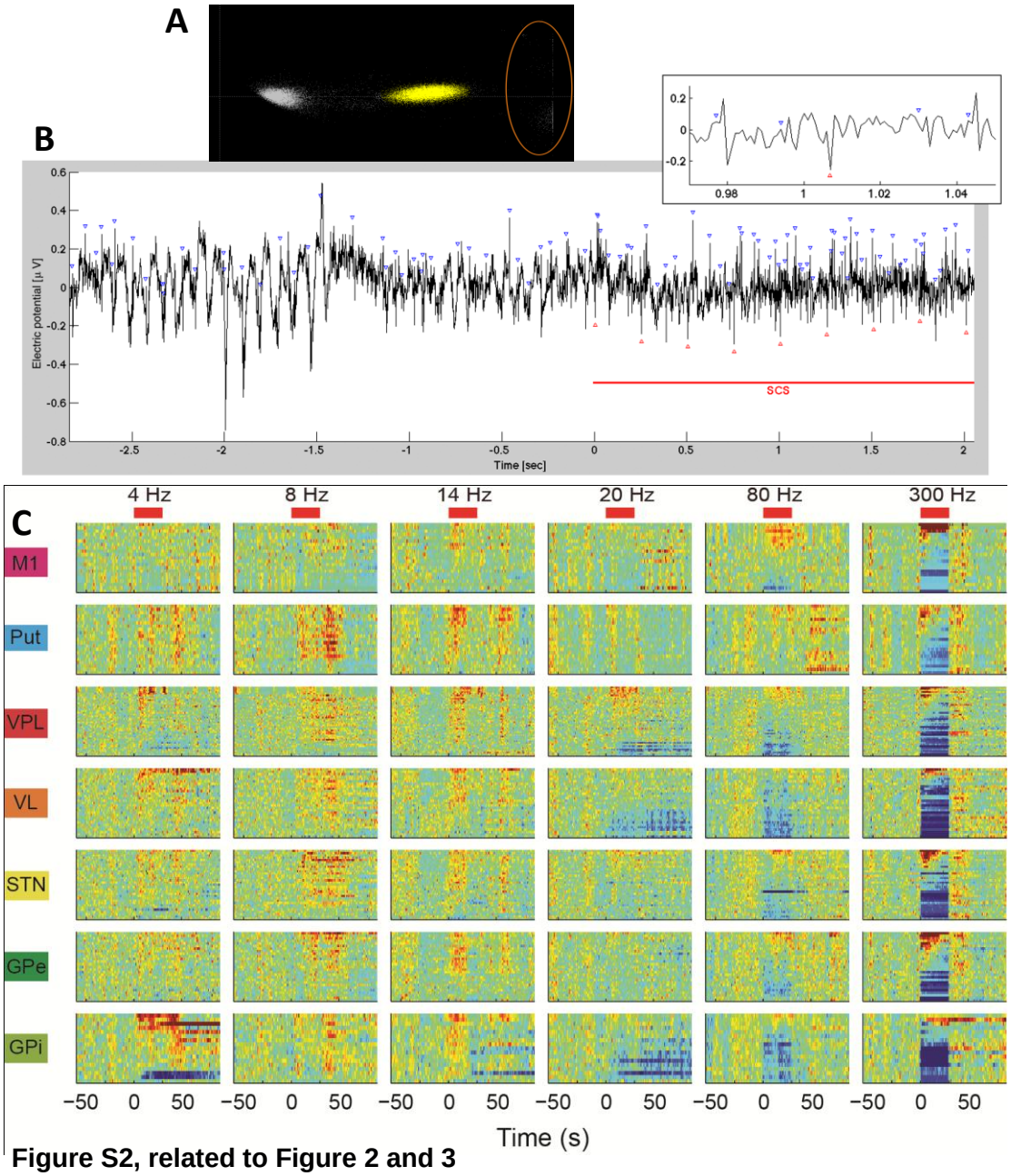

Figure S2, related to Figure 2 and 3

(A,B) Reliable spike and LFP recordings during SCS ON periods were obtained following off-line removal of stimulation artefacts. (A) Off-line removal of stimulation artefacts was performed based on clear differences to normal spike-morphology as well as the coincident detection in several recording channels (stimulation artifacts are encircled to the right whereas the yellow cluster represents a single unit recorded concurrently in the same channel). **(B)** Example of a low-pass filtered (<300 Hz) voltage trace. Timestamps for SCS pulses were extracted from a trigger channel and are marked here with red triangles. Timestamps of unit spike activity were extracted from the wide-band signal as in A and are marked here with blue triangles for comparison. SCS artifacts were often clearly visible in the low-pass filtered traces, but were well confined to a few milliseconds around each pulse. Note that the firing rate of the identified neuron is in this case relatively unaltered as the SCS is turned on at t=0. It is also interesting to note that parkinsonian LFP beta-oscillations are distinguishable prior to SCS on-set even in the raw data trace. **(C)** Time extended version of Figure 3A showing the firing rate modulation after the SCS period (red bar) at different stimulation frequencies.

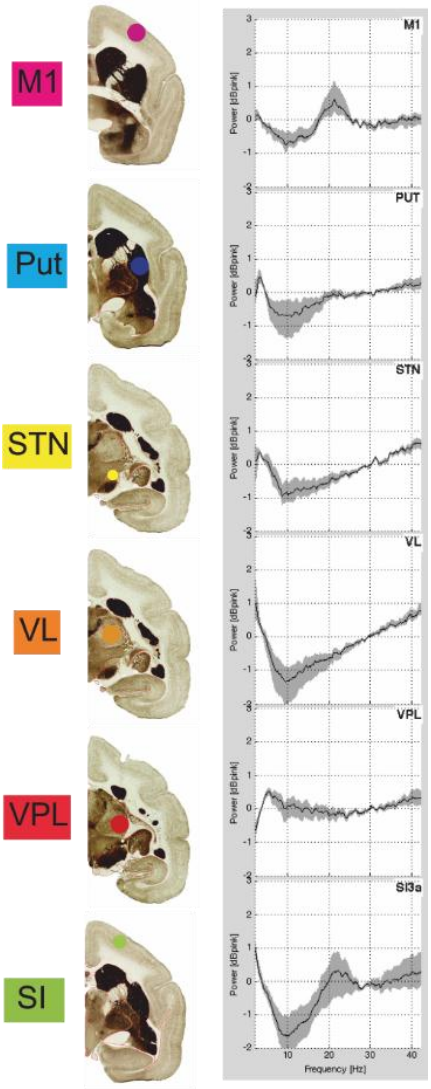

Figure S3, related to Figure 2 and 3

(A) The intact animal showed no increase in LFP beta-power. In control experiments LFP power spectra were obtained from an intact animal. Average LFP power spectra from an example recording normalized to the pink noise background are shown for the different structures (shaded area denotes the bootstrap-estimated confidence interval of all the electrode pairs in each structure). Note that no indication of exaggerated LFP beta-power can be found in any of the recorded structures. **(B) Spinal cord stimulation causes physiological changes resembling the effect of levodopa treatment.** Histograms showing the quantitative resemblance to the intact hemisphere (4 left panels) and the L-DOPA treated condition (4 right panels), respectively, for each 4s-epochs of the SCS recordings (SCS OFF=black and SCS ON=red). Lighter colors (gray, pink) denote periods of motor activity, while dark colors (black, red) are periods where the animal did not move. Note that while an active behavioral state in parkinsonian animals significantly shifted firing rate and LFP spectral contents towards the intact/L-DOPA treated state, this effect was much smaller than the SCS-induced LFP changes (effect-sizes, as fraction of total variance explained, eta-squared, is given under each pair of histograms OFF/ON; two-way ANOVA).

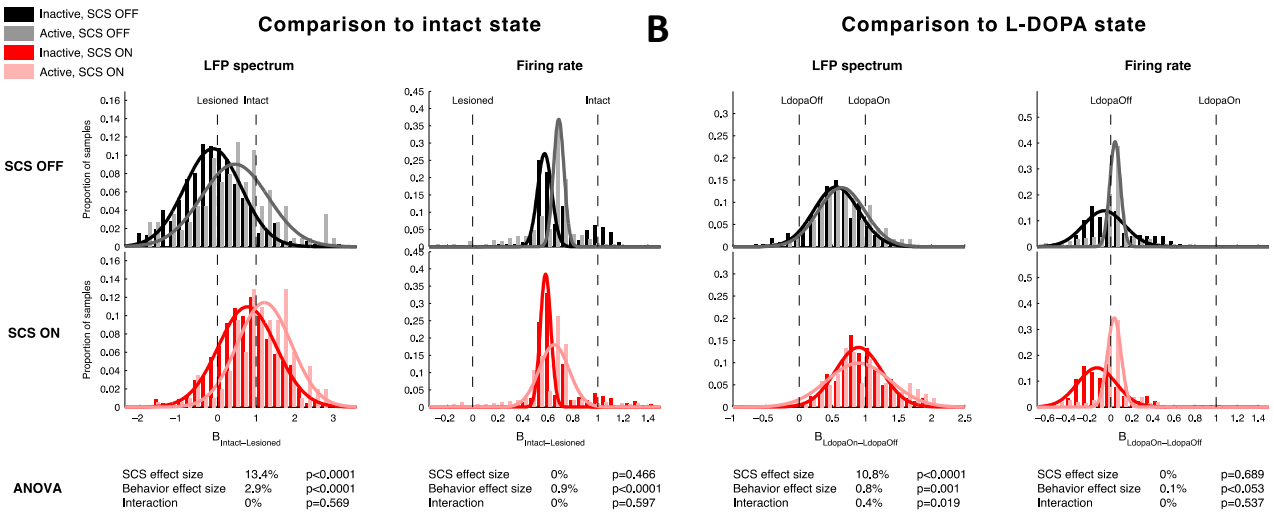

A

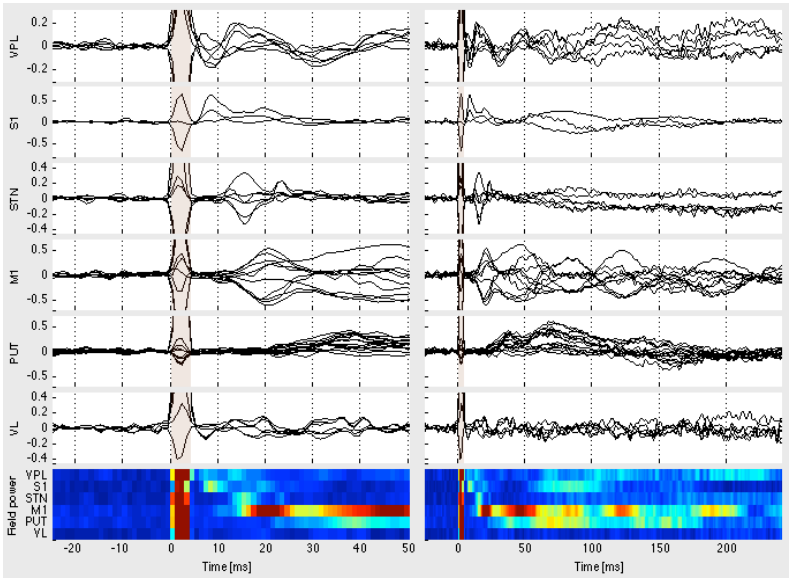

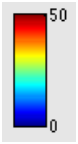

	Onset	Peak
VPL	<5	6-7
S1	6	8
STN	11	15
M1	13-14	20
PUT	21	37
VL	<6?	7?

B

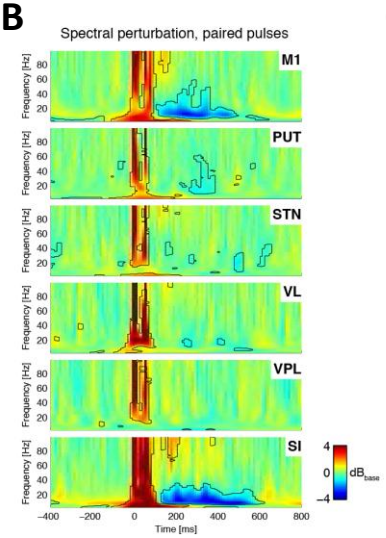

C

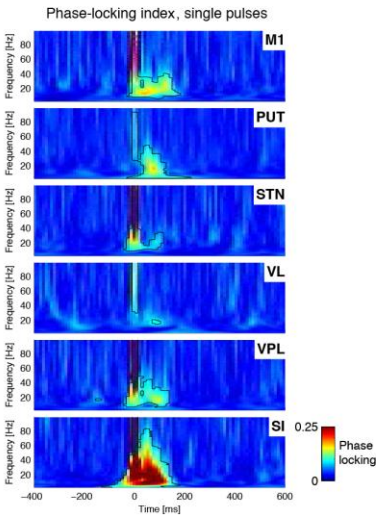

D

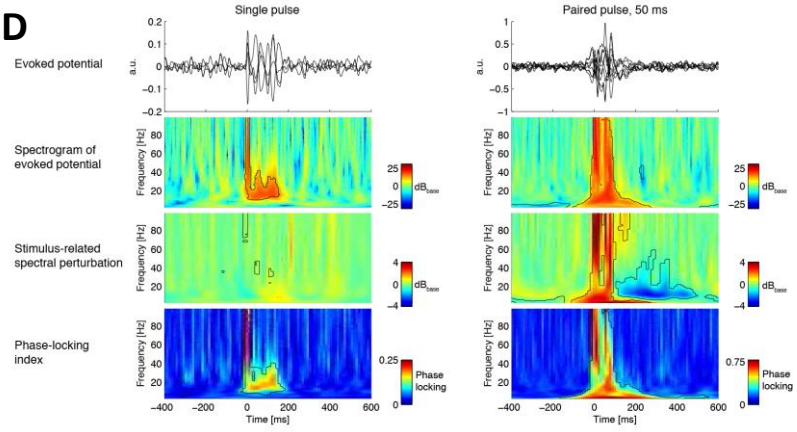

E

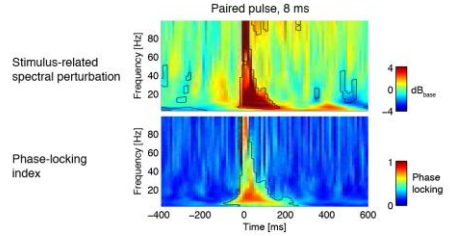

Figure S4, related to Figure 2, 3, and 4

(A) Evoked potentials following single SCS pulses suggest direct activation of primary somatosensory structures via the dorsal column-medial lemniscal pathway. Average responses following a single SCS pulse (n=1000 pulses delivered at 1 Hz). The left and the right columns show the same data, but with different time resolution (left column: -20 to +50 ms and right column -20 to 250 ms). Earliest neuronal responses were recorded in the VPL thalamic nucleus (top row) followed by the S1 cortex (second row). The shaded area from 0 to 4 ms indicates the stimulation artifact. Each trace shows the normalized difference in electric potential between two electrodes in the same structure. The bottom row shows the standard deviation across all traces from the same structure, normalized to the standard deviation of the baseline ('standardized field power'). This quantity can be interpreted as a consolidated measure of activation in a given structure. Approximate onset and peak latencies are summarized in the table to the right.

(B, C) Stimulation phase-locks LFP-oscillations to each stimulation pulse and desynchronizes cortical beta-oscillations. **(B)** Spectrograms showing the average change in LFP-power resulting from pairs of SCS pulses separated by 50ms (stimulus-related spectral perturbation). Warm colors indicate an increase relative to pre-stimulus baseline, while cool colors indicate a decrease. Black isolines indicate p=0.01 (bootstrap). Paired pulses strongly suppressed beta oscillations in sensory and motor cortex (blue areas around 300 ms). **(C)** Phase-locking index shown as a function of frequency and time for repeated single-pulse stimulations (an index of 1 means that the phase is identical in all trials, while 0 means that the phase is random). While single pulses did not suppress low-frequency oscillations an abrupt phase-reset that resulted in phase-locked beta-oscillations up to 200 ms after an incoming pulse was observed in several structures.

(D, E) Desynchronization of beta oscillations through destructive LFP-interference. **(D)** Motor cortex responses to single pulses (left column) and paired pulses with 50ms inter-pulse interval (right column) as measured by evoked potentials (top row), spectrograms of the evoked potentials (second row), stimulus-related spectral perturbations (third row) and phase-locking indices (bottom row). Black isolines in heat maps indicate p=0.01 (bootstrap). An increase in the beta band can be seen in the evoked potential of the single pulse (first and second row, left column). This increase is a result of the phase-locking seen in the left, bottom row, since there is no corresponding increase in the beta power calculated from the unaveraged traces (third row, left column). By contrast, two pulses with 50ms spacing induce a beta power suppression that persists for several hundred milliseconds (third row, right column). **(E)** The paired pulse desynchronization effect is not obtained when using an IPI of 8 ms, which is substantially shorter than half the period of the beta oscillation. Together this suggests that the observed beta suppression is a result of destructive interference between oscillations with opposite phase.

Supplemental Experimental Procedures

Animals

Five adult male common marmosets (*Callithrix jacchus*) 300-550g were used. The animals were housed in pairs in cages (1.0 x 1.0 x 2.3 m) in a vivarium with natural light cycle (~12/12 hours) and outdoor temperature and humidity. All animal procedures were carried out according to approved protocols by AASDAP Ethics Committee and strictly in accordance with the National Institute of Health Guide for the Care and Use of Laboratory Animals (NIH Publications No. 80-23). This project was approved by SISBIO/Brazilian Institute of Environment and Natural Resources under No. 20795-2.

Symptoms observed in the parkinsonian marmosets

(1) Hypokinesia: a general reduction in motor activity (motility, grooming, climbing, vocalizing)
(2) Bradykinesia – noticeable slowing of the execution of movements
(3) Episodes of freezing – brief periods of sudden immobility when initiating quadripedal locomotion or goal directed reaching
(4) Uncoordinated gait – inaccurate positioning of the limbs and wobbling of the trunk during locomotion (in the literature referred to as clumsy, poor-balanced gait; Eslamboli, 2003).
(5) Difficulty in changing to bipedal stance – noticeable in the reaching task, when, in order to reach the food present in higher positions, the task requires a bipedal posture.
(6) Akinesia - long periods (up to 30 seconds) with complete lack of spontaneous motor activity in awake animals.
(7) Rigidity – particularly noticeable in forelimbs during extension.
(8) Slowed alarm response – animal would not respond to vocal alarm signals from other mates (only occasionally observed)
(9) Slowed climbing – observed in home cage. Analogous to locomotion on ground but often more pronounced (when slowing of locomotion was observable only in climbing, bradykinesia was classified as moderate)
(10) Balance - difficulties to maintain a resting position supported on four limbs while on tree branches
(11) Episodes of hypomimia – reduction of the marmoset's typical behavior of maintaining eye contact and impaired inability to display facial expression in response to interaction with care givers
(12) Ipsilateral head position bias in relation to lesion - noticeable during the first few weeks after lesions
(13) Reduced fine motor skills - difficulty in reaching and grasping small food objects

(14) Reduced gross motor skills – difficulties in grasping branches (less commonly observed)

Manual assessments of motor disability

Motor disability during recording sessions when the animal was placed in the transparent acrylic chamber was scored by an observer blinded to treatment conditions using a rating scale adapted for the common marmoset (Bankiewicz et al., 2001; Fahn and Elton, 1987; Hansard et al., 2002). Eight different symptoms were rated according to four levels of severity ranging from no occurrence [0] to maximum severity [3], except fine and gross motor skills [0-6] and bradykinesia [0-9]. The rated symptoms were:

Freezing
[0]: Unhindered to move the body and show normal use of the limbs, e.g., in finding and grasping marshmallows in the reaching task
[1]: Difficulties in starting to walk, or in the initiation of particular movement when walking. For example, when reaching for a marshmallow, the start of the reaching movement is delayed. In these cases the freezing episodes are short.
[2]: Same as in [1], but the freezing episodes have a longer duration - between 5 and 10 seconds.
[3]: Same as in [1], but freezing episodes last over 10 seconds.

Gait and locomotion
[0]: Walks normally according to its pre-lesion locomotion patterns, with symmetrical limb use.
[1]: Shows reduced walking activity and walks with mild asymmetry.
[2]: Walks slowly, with asymmetry, and occasionally drags a limb (usually a hindlimb).
[3]: Unable to walk

Fine motor skills (scored for each arm independently)
[0]: Normal ability to grasp marshmallows.
[1]: Grasps with difficulty.
[2]: Grasps with difficulty and requires one arm to support the stance while using the other to grab the marshmallow.
[3]: Totally unable to grasp marshmallows.

Bradykinesia (scored independently for limbs and trunk)
[0]: No difficulty in initiating or performing rapid and precise movements.
[1]: Difficulties in initiating movements and displays smoother and slower movements when reaching for marshmallows or moving around in the box spontaneously
[2]: Clear delay in initiating movements and shows a marked slowing of movements in reaching and in spontaneous motor activity in the box
[3]: Totally immobile

Hypokinesia
[0]: moves freely and is alert and responsive
[1]: reduced activity, moves with less speed

[2]: low spontaneous activity, moves when provoked
[3]: Totally immobile

Coordination and body balance
[0]: normal stance and coordination
[1]: compromised coordination but changes from quadrupedalism to bipedalism, without falling
[2]: compromised coordination, unstable locomotion with occasional falls
[3]: face down or lying in supine position unable to maintain any kind of stance.

Posture
[0]: normal posture
[1]: somewhat altered posture when standing such as wider positioning of limbs, resting with limbs and tail in abnormal body position
[2]: hunched posture, abnormal trunk position; abnormal head posture (neck flexed or inclined to one side)
[3]: unable to maintain posture, lying in the supine or lateral position

Gross motor skills (scored for each arm independently)
[0]: normal limb use when grasping larger objects
[1]: reduced ability to grasp larger objects to support body weight
[2]: rarely is able to grasp larger objects to support body weight
[3]: unable to grasp and hold large objects/structures;

To eliminate any inter-individual variability, the rating of the symptoms of each animal was done in comparison to the motor performance of that individual prior to lesioning. In the summed PD-score each symptom was normalized separately to its maximum severity score. Assessments were first performed six hours after systemic AMPT-treatment and continued during the following spinal cord stimulation experiment.

Automatic quantification of motor activity

Spontaneous motor behavior was recorded in a transparent acrylic chamber to which the animals had been previously habituated. Locomotion and general motility was automatically quantified from digital video recordings obtained from two orthogonally positioned cameras. Custom written Matlab code was used to calculate movements from the videos. A measure of general motility was computed from the changes in pixel intensity in successive image frames. The motility index was then defined as the fraction of video frames with more than 150 significantly changed pixels (approx. 6 cm^2). To quantify motion bouts an ellipsoid was projected and fitted to the foreground area in the respective camera images, enclosing the torso. Translational movements of the ellipsoid in 3D were used to estimate frame-to-frame velocities during locomotion bouts.

Statistical analyses of locomotor behavior

To test for significant differences in locomotor behavior the following statistical tests were applied:
Motility – the average motility during each condition was calculated for each recording session and was then compared using a paired non-parametric test (Wilcoxon signed rank).
Bout frequency – the proportion of time periods containing locomotor activity was compared using a two-proportion z-test.
Bout duration and distance – individual bouts were pooled from all recording sessions and the duration and distance of the individual bouts were compared between conditions using a non-parametric unpaired test (Wilcoxon rank sum).
In the case of multiple comparisons on the same measure between conditions pairs (Fig. S3) these tests were preceded by an appropriate omnibus test (Motility: Friedmans, Bout frequency: Chi-square, Bout duration and distance: Kruskal-Wallis).
Analyses of significance were performed using either Matlab functions or GraphPad Prism 5.04 software.

Surgical procedures

All surgical procedures were carried out under antiseptic conditions. Animals were initially sedated with ketamine (10-20 mg/kg i.m.) and Atropine (0.05 mg/kg i.m.) followed by deep anesthesia with isoflurane 1-5% in oxygen at 1-1.5 L/min during the surgery.

6-OHDA lesions

Two microliters of 6-OHDA solution (4 mg/mL, 0.05% ascorbic acid, saline) was injected with a 32 gauge syringe at 0.5 µL/min into the medial forebrain bundle in the following five locations (interaural AP/ML/DV): 6.5/1.2/6.0; 6.5/1.2/7.0; 6.5/2.2/6.5; 6.5/2.2/7.5; 6.5/3.2/8.0 (modified from Annett et al. 1992). Anteroposterior coordinates were corrected according to the dimensions of the skull of each animal (Stephan et al., 1980). Following surgery, the animals received non-steroid anti-inflammatory analgesic (flunixin meglumine 1mg/kg, s.c.) for 3 days, dexamethasone (0.5 - 1mg/kg, i.m.) for 5 days and enrofloxacin (5 mg/kg, s.c.) for 7 days. The same procedures were used for the second contralateral lesion and after the implantation of recording arrays and stimulation electrodes.

Recording electrodes

Six small holes were drilled in the cranium for insertion of stainless steel screws used to secure the implant and serve as ground connections for later recordings. Two craniotomies for the electrode arrays in each hemisphere were then performed. Meninges were carefully removed and the cortical surface was kept wet using sterile gauze soaked with saline solution. Electrodes were stereotactically implanted using a micromanipulator targeting the following coordinates (interaural AP/ML/DV): MI: 10.0/6.5/14.4; SI: 8.0/5.2/15.6; Put: 8.5/6.5/11.5; GPi: 8.0/3.5/7.8/13.2; GPe: 8.0/5.2/8.8/12.2; VL: 5.5/3.7/10.5; VPL: 4.5/4.3/9.2; STN: 5.5/3.7/7.6. After implantation, electrodes and connectors were fixed to the skull with dental acrylic.

Stimulation electrodes

Stimulation electrodes were implanted 2 weeks after the recording electrodes. Through blunt dissection, the spine was exposed at T3-T4. After laminectomy of the T3 vertebra, a two-plate platinum electrode (each 1x3 mm with a 0.5 mm spacing) was inserted at the T3-T4 spinal level, placed longitudinally in the epidural space over the dorsal spinal cord. The wires from the stimulation electrode were then passed subcutaneously to a connector positioned next to the recording implant on the skull.

Spinal cord stimulation procedures

For SCS, biphasic charge balanced square pulses (each pulse either 200 or 400 us in duration separated by 100 us) were applied using an 8-channel general-purpose stimulus generator (STG4008, Multichannel Systems MCS GmbH) . For each frequency (4, 8, 14, 20, 80, 125, 300 Hz) the minimum intensity where any behavioral response (typically, a small postural change in response to the on-set of the stimulation) could be observed was established before each testing session. Stimulation thresholds varied greatly between subjects (100-1600 uA) but showed a consistent relationship to stimulation frequency in the sense that higher frequencies required lower stimulation intensities. SCS sessions were conducted at 1.7 times the threshold intensity.

Pharmacological treatment

Six hours prior to recording experiments the animals received an injection of alpha-methyl-para-tyrosine (AMPT; 120 mg/kg, s.c.) which was repeated 3 hours later, resulting in a total dose of 240 mg/kg. In experiments evaluating the effect of L-DOPA, animals were injected with 15 mg/kg L-DOPA/ 6,25mg/kg Benserazide, s.c. in saline solution during light isoflurane anesthesia.

Signal acquisition

Local field potentials and unit activity (spikes) were acquired using an OmniPlex D Neural Data Acquisition System (Plexon Inc.). The signal from the headstage pre-amplifier (6x gain, Nicolelis/Duke Headstage) was amplified between 4800 and 153000 times, high-pass filtered with cut-off 0.5 Hz, and digitized at 16 bits and 40 kHz. To obtain the local field potentials, the signal was low-pass filtered with a cut-off frequency of 300 Hz and down-sampled to 1000 Hz. To obtain the spikes, the signal was high-pass filtered with a cut-off frequency of 600 Hz. Subsequently, 0.8-ms epochs around samples greater than 2.5 times the signal-noise were saved for off-line sorting.

Frequency analysis of LFPs

After standardization of the raw LFP time series, local bipolar LFP time series were computed offline from all unique pairs of electrodes from the same structure. Occasional artifact periods were detected and rejected with a flatness criteria (thresholding of the median of the absolute value of the sample-to-sample difference). Power spectral densities (PSDs) were calculated with a multitaper method (Pesaran, 2008) (50%-overlapping 8-s windows, 7 tapers) implemented in Chronux 2.0 (Mitra and Bokil, 2007). Frequency-specific artifacts such as power line noise (60 Hz) and stimulation artifacts were removed from the PSDs (+/- 1 Hz and also removing harmonics). PSDs were normalized to the pink noise background according to (Halje et al, 2012), using the frequency bands 2-6 Hz and 20-120 Hz for the pink noise estimation. This allowed us to describe PSD deviations from the pink noise floor conveniently in terms of the unit dB_{pink}. All PSDs belonging to the same recording session, channel and treatment state (e.g. SCS off or on) were averaged. This data was finally pooled across sessions and the within-structure average and confidence intervals were calculated (bootstrap, 100 permutations).

Time-frequency spectrograms (Fig. 2a) were calculated in the same manner, except that the window size was 4 seconds with a 75% overlap and there was no averaging over time.

The stimulus-related spectral perturbation (SRSP) and phase-locking index (or inter-trial coherence; ITC) as shown in Fig S4 were calculated with the EEGLAB toolbox (Delorme and Makeig, 2004). The window length was scaled with the frequency ('wavelet analysis') so that the length was always two cycles, e. g. 100 ms at 20 Hz. The pad ratio was set to four, which resulted in an apparent frequency resolution of 0.67 Hz. SRSPs were normalized to a pre-stimulus baseline and expressed in decibels. The pre-stimulus baseline was defined as the average of all PSDs with a window centered between 250 ms and 50 ms before the stimulus. Note that the ITC values were not baseline corrected; an index of 1 means that the phase is identical in all trials, while 0 means that the phase is random.

Coherence and estimation of functional connectivity

After local bipolar re-referencing (see above, section Frequency analysis of LFPs), the coherence was computed between all pairs of simultaneously recorded LFP signals. In detail, a multitaper method (Pesaran, 2008) (non-overlapping 3-s windows, 5 tapers) implemented in Chronux 2.0 (Mitra and Bokil, 2007) was employed to estimate the multitaper Fourier transforms $\mathrm{X_{i,n}(f)}$, where i and n are indices for the individual LFP signals and time windows, respectively. The coherence was then estimated to

$$C_{ij}(f) = \frac{S_{ij}(f)}{\sqrt{S_{ij}(f)S_{ij}(f)}}$$

with

$$S_{ij}(f) = \frac{1}{N}\sum_{n=1}^{N} X_{i,n}(f)\, X_{j,n}^{*}(f)$$

where the asterisk denotes complex conjugation and *N* is the number of windows to be averaged over. For LFP signals recorded in L-dopa experiments (contributing to intact, L-dopa, and Parkinsonian coherences), the average was taken over 10 windows, resulting in a time resolution of 30 s for the coherence. For LFP signals recorded in the SCS experiments (contributing to SCS On and Parkinsonian coherences), the average was taken over all windows obtained in the time period during and immediately preceding every stimulation trial, respectively. Pairs of LFP signals whose coherence measures systematically showed an abnormally strong coherence over all frequencies, indicating the presence of a common signal despite previous re-referencing, were excluded via visual inspection.

Because several recording electrodes were used in each structure, there were also several coherence measures for each pair of structures (i.e., one measure for each pair of LFP signals). In order to obtain one mean coherence for each pair of structures, the mean magnitude-squared coherence (MSC) was calculated employing the variance-stabilizing transform for the coherence (arc-tanh)(Pesaran, 2008). Denoting the coherence measures between structures *X* and *Y* by $C_{XY}^{(i)}(f)$, with $i = 1, \dots, N_{XY}$, the corresponding mean MSC becomes $\overline{MSC}_{XY}(f) = \left|\tanh \frac{1}{N_{XY}} \sum_{i=1}^{N_{XY}} \tanh^{-1}\left|C_{XY}^{(i)}(f)\right|\right|^2$.
The resulting mean MSCs were then integrated over the 8-15 Hz range as well as the 30-40 Hz range, and the corresponding ratio was calculated. The Wilcoxon rank sum test was employed to test for significant differences between the distributions of these ratios.

Evoked potentials

After standardization of the raw LFP time series, local bipolar LFP time series were computed offline from all unique pairs of electrodes from the same structure. Evoked potentials were calculated with respect to the onset of each pulse (the first pulse when paired pulses were used). The data was baseline corrected, i.e. the DC of the baseline period was removed, for each epoch before averaging. The baseline period was set to 0-25 ms before the stimulus.

To get a consolidated measure of activity in a structure, we calculated the 'standardized field power' as follows. First, we calculated the standard deviation across all channels in a structure:

$$y(t) = \sqrt{\frac{\sum_{i=1}^{N}(x_i(t) - \langle \boldsymbol{x}(t)\rangle)}{N}}$$

where x_i is the LFP time series of channel *i*, *N* is the number of channels in the structure and angle brackets denote the average across channels. Second, we normalized *y* to the standard deviation of the baseline and obtained the standardized field power

$$y'(t) = y(t)/\mathrm{std}(\boldsymbol{y}_{\mathrm{base}})$$

where

$$\boldsymbol{y}_{\text{base}} = \{y(t),\ \ t \in [-25\ \text{ms}, 0\ \text{ms}]\}$$

In Fig S4D (panel A, second row) we show spectrograms of evoked potential. These spectrograms were generated with the same methods and settings as the SRSPs in the third row, but from averaged traces (the EPs in the top row) instead of from the raw traces.

Spike sorting

Spike trains were cleaned for cross-channel artefacts (events that occurred within 200 us in at least 10% of channels) and high amplitude artefacts (>900 uV) using Offline Sorter (version 3.3.2; Plexon Inc.). Waveforms were clustered automatically with slightly modified algorithms from the Chronux toolbox(Fee et al., 1996). All automatically generated clusters were manually reviewed to determine if clusters, waveforms and interspike-interval distributions were physiologically plausible. Clusters were only modified by merging and splitting them according to the cluster hierarchy imposed by the algorithm.

Spike train beta-power calculation

For each unit, the spike timestamps from either the SCS OFF or SCS ON epochs across the entire session were identified, merged, and fed to the function *pxcorr* (Chronux toolbox) (Mitra and Bokil, 2007) with a bin size of 5 ms and a maximum lag of 0.5 s. The resulting autocorrelogram was normalized by the total number of spikes, the central bin equated to zero and the average subtracted to finally compute the PSD. To assess significant rhythmicity in the beta range, 100 pseudorandom spike trains with the same average firing rate were created and the PSD computed the same way. A unit was deemed as having significant beta activity if the sum of the PSD in the range 8-16 Hz was greater than the highest 99% of the PSD obtained from pseudorandom spike trains. To assess significant differences in the beta power between the OFF and ON conditions, the ratio between the PSD-OFF and PSD-ON in the 8-16 Hz range was calculated. This was compared to the highest 99% of the ratios computed by pseudorandom permutation of the two PSD sets created in the previous step from the pseudorandom spike trains. Since this method was based on a pseudorandom process, units with borderline significant differences could appear as significant or not, as the analysis was repeated. To solve this, the entire analysis was repeated 100 times and the average result was reported.

Describing similarity to intact and levodopa states through an LFP/firing rate benchmark index

Definition of the benchmark index:

Let the row vector **x** represent any sampled data point, while $\mathbf{x}_{\mathrm{I}}$ and $\mathbf{x}_{\mathrm{II}}$ each represent a data point from state I and state II, respectively. Let $\langle \boldsymbol{x}_{\mathrm{I}} \rangle$ denote the average of all samples belonging to state I. The mean difference between the states,

$$\boldsymbol{b} = \langle \boldsymbol{x}_{\mathrm{II}} \rangle - \langle \boldsymbol{x}_{\mathrm{I}} \rangle ,$$

can be interpreted as a direction in the space of all measured variables, and by taking the scalar product $\boldsymbol{x} \cdot \boldsymbol{b}$ we get the projection of any sample **x** onto this direction. Hence, we could construct a benchmark index

$$B_{\mathrm{II-I}}(\boldsymbol{x}) = \frac{(\boldsymbol{x} - \langle \boldsymbol{x}_{\mathrm{I}} \rangle) \cdot \boldsymbol{b}}{\|\boldsymbol{b}\|^2}$$

with the intuitive geometrical interpretation of being the projection onto the mean state difference, while fulfilling $B_{\mathrm{II-I}}(\langle \boldsymbol{x}_{\mathrm{I}} \rangle) = 0$ and $B_{\mathrm{II-I}}(\langle \boldsymbol{x}_{\mathrm{II}} \rangle) = 1$.

Description of what was benchmarked

We created benchmark indices for two state comparisons: $B_{\mathrm{OnLD\text{-}OffLD}}$ for comparing the levodopa treated state with the untreated disease state, and $B_{\mathrm{Intact\text{-}Lesioned}}$ for comparing the healthy state to the untreated disease state. These benchmarks were then applied to the SCS data set (including SCS OFF periods) so that we obtained the four distributions

$$B_{\mathrm{OnLD-OffLD}}(\boldsymbol{x}_{\mathrm{OnSCS}})$$

$$B_{\mathrm{OnLD-OffLD}}(\boldsymbol{x}_{\mathrm{OffSCS}})$$

$$B_{\mathrm{Intact-Lesioned}}(\boldsymbol{x}_{\mathrm{OnSCS}})$$

$$B_{\mathrm{Intact-Lesioned}}(\boldsymbol{x}_{\mathrm{OffSCS}})$$

Two types of data vectors were used: population firing rates and LFP power spectra. For firing rate data, each data point consisted of the per-structure population firing rate from a 4 s time window (a 7-element vector). For LFP data, each data point was the concatenation of the power spectra from the seven structures from a 4 s time window. In addition, the SCS data was split in two sets based on motor activity/inactivity. Together, this gave us the 16 *B*-distributions displayed in Figure S3B. All data was preprocessed with standard PCA methods (Matlab) to reduce dimensionality and noise.

Histology

Tissue preparation

Under deep ketamine anesthesia [ketamine (40 mg/kg i.m.) + xylazine (0.04 mg/kg i.m.) + atropine (0.05 mg/kg i.m.)] the animals were intracardially perfused with physiological saline, followed by 4% ice-cold paraformaldehyde. The brains were post-fixed in the same solution for 2h, transferred to 20% followed by 30% sucrose in 0.1 M phosphate buffer saline for 12h. Brains were frozen in an embedding medium (Tissue Tek) and were then sectioned frontally at 50 µm thickness in a cryostat (Carl Zeiss Micron, HM 550, Germany). The sections were mounted on electrically charged glass slides (SuperFrost Plus - Fisher Scientific International) for further histological processing.

Sections were pre-incubated in a 1% hydrogen peroxide solution in methanol for 20 minutes to remove endogenous peroxidase activity. Sections were then rinsed in 0.05% phosphate buffer-Tween 0.05% (PB-T) for 5 minutes and incubated in 10% goat normal serum (diluted in 0.1M PB; Vector Laboratories) for 30 minutes in order to block non-specific binding. After that, sections were incubated in primary antibody against TH (rabbit polyclonal antibody; 1:500; diluted in normal serum; Merck Millipore) overnight at room temperature in a humidified chamber to prevent air-drying. Sections were washed in PB-T 1% for 5 minutes. The sections were then incubated with a biotinylated goat anti-rabbit secondary antibody (1:200, diluted in PB; Vector Laboratories) for 2h, washed for 5 minutes in PB-T, and then incubated in avidin-biotin-peroxidase solution (Vectastain Standard ABC kit) for 1h. After washes in PB, slides were placed in a solution containing 0.03% 3,3'-diaminobenzidine tetrahydrochloride hydrate (DAB) (Sigma) and 0.001% hydrogen peroxide in 0.1M PB. Finally, the sections were washed and the slides left to dry overnight. After dehydration through a series of graded alcohols and clearance in xylene, the slides were cover-slipped using Entellan (Merck) mounting medium.

Quantification of striatal fiber density and dopaminergic midbrain cells through TH-immunoreactivity

Tissue samples were mounted and pictures were taken using a microscope with the same camera configuration and identical illumination conditions. TH-reactivity in both caudate-putamen and SNc/VTA was quantified by computer densitometry. Digital images were collected using a CX9000 camera (MBF Bioscience Inc.), attached to a light field Nikon Eclipse 80i optical microscope (10x and 20x objectives). TH reactivity across caudate-putamen was assessed by optical densitometry using ImageJ software (http://rsb.info.nih.gov/ij/). Measurements were obtained by using a 0.2 mm^2 window positioned in different striatal regions (60 regions per striatum and animal). The TH reactivity of the internal capsule (averaged over measurements of 10 different sites using the same window) was used to set the lower boundary of the staining scale in each sample.

Prior to quantification of cells labelled by TH-IR, the borders of SNc were defined using Paxinos Atlas (2012). A fixed area of the SNc was used to compare anterior, central and caudal areas. Area estimates and cell counts were obtained using the StereoInvestigator system (MBF Bioscience Inc.). At least three sections were analyzed per animal.

Supplemental References

Annett, L.E., Rogers, D.C., Hernandez, T.D., and Dunnett, S.B. (1992). Behavioural analysis of unilateral monoamine depletion in the marmoset. Brain *115 (Pt 3*, 825–856.

Bankiewicz, K.S., Sanchez-Pernaute, R., Oiwa, Y., Kohutnicka, M., Cummins, A., and Eberling, J. (2001). Preclinical models of Parkinson's disease. Curr. Protoc. Neurosci. *Chapter 9*, Unit9.4.

Delorme, A., and Makeig, S. (2004). EEGLAB: an open source toolbox for analysis of single-trial EEG dynamics including independent component analysis. J. Neurosci. Methods *134*, 9–21.

Fahn, S., and Elton, R.L. (1987). Unified Parkinsons Disease Rating Scale. Recent Dev. Park. Dis. *2*, 153–163.

Fee, M.S., Mitra, P.P., and Kleinfeld, D. (1996). Automatic sorting of multiple unit neuronal signals in the presence of anisotropic and non-Gaussian variability. J. Neurosci. Methods *69*, 175–188.

George Paxinos, Charles Watson, Michael Petrides, Marcello Rosa, H.T. (2012). The Marmoset Brain in Stereotaxic Coordinates. (Academic Press)

Halje, P., Tamtè, M., Richter, U., Mohammed, M., Cenci, M.A., and Petersson, P. (2012). Levodopa-induced dyskinesia is strongly associated with resonant cortical oscillations. J. Neurosci. *32*, 16541–16551.

Hansard, M.J., Smith, L.A., Jackson, M.J., Cheetham, S.C., and Jenner, P. (2002). Dopamine, but not norepinephrine or serotonin, reuptake inhibition reverses motor deficits in 1-methyl-4-phenyl-1,2,3,6-tetrahydropyridine-treated primates. J. Pharmacol. Exp. Ther. *303*, 952–958.

Mitra, P., and Bokil, H. (2007). Observed Brain Dynamics (Oxford University Press, USA).

Pesaran, B. (2008). Neural Signal Processing: Quantitative Analysis of Neural Activity. Soc. Neurosci. 1–12.

Eslamboli, A., Baker, H.F., Ridley, R.M., and Annett, L.E. (2003). Sensorimotor deficits in a unilateral intrastriatal 6-OHDA partial lesion model of Parkinson's disease in marmoset monkeys. Exp. Neurol. 183, 418–429.

Stephan, H. , Baron, G., and Schwerdtfeger, W.K. (1980). The brain of the common marmoset (Callithrix jacchus) : a stereotaxic atlas. (Springer)

Movie legends

Movie S1, examples of Parkinsonian motor deficits in marmosets, related to Figure 1

The first part of the video shows motor deficits in a unilaterally lesioned marmoset engaging in a reaching task designed to force the animal to use the impaired forelimb (right side in this animal). The last part shows an example of a freezing episode involving the whole body during spontaneous locomotion behavior in a bilaterally lesioned animal.

Movie S2, example of SCS effect, related to Figure 1

The video shows an example of dramatic recovery of motor functions in a severely parkinsonian animal during SCS. Notably, from a state of complete akinesia, a clearly goal-directed behavior is displayed as the animal searches and retrieves food rewards during the SCS ON period. Shortly after the off-set of SCS the animal once again returns to complete akinesia.